

A New Method for Diagnosing Patients Suspected of Bone Marrow Metastasis in the Presence of Outliers

Mahmood Shahrabi ^a, Amirhossein Amiri ^{*b}, Hamidreza Saligheh Rad ^c, Sedigheh Ghofrani ^d

^a Department of Industrial Engineering, South Tehran Branch, Islamic Azad University, Tehran, Iran

^b Department of Industrial Engineering, Faculty of Engineering, Shahed University, Tehran, Iran

^c Department of Medical Physics and Biomedical Engineering, Tehran University of Medical Sciences, Tehran, Iran

^d Department of Electrical and Electronic Engineering, South Tehran Branch, Islamic Azad University, Tehran, Iran

Received 03 January 2021; Revised 15 November 2021; Accepted 18 November 2021

Abstract

In recent years, medical images have played an essential role in diagnosis, treatment, and training areas. Thus, any advancement in this field can help doctors in diagnosing. On the other hand, statistical process control (SPC) is now widely used in monitoring healthcare processes. In this research, using the image processing techniques and feature extraction methods (two-dimensional discrete wavelet), we propose some multivariate control charts to diagnose the type of bone marrow of the patients suspected of bone marrow metastasis in the pelvic region with early breast tumors. For this, 76 features (energy and histogram of oriented gradient) are extracted from the image. Next, using the GA, six features are selected and constitute a feature vector. Based on the feature vector, the Hotelling's T^2 multivariate control charts are developed. Moreover, considering the high sensitivity of the classic estimators to outliers and contaminated data, we provide a robust Hotelling's T^2 control chart. Finally, we compare the ARL performance of the robust and the classic Hotelling's T^2 control charts in Phase II in the presence of local outliers in the Phase I data. The results confirmed the superiority of the robust version.

Keywords: Robust Hotelling's T^2 control chart; Average run length; Feature extraction; Bone marrow metastasis

1. Introduction

Hotelling's multivariate T^2 control chart is one of the most popular multivariate control charts. For the design of this chart, the estimation of the mean vector and variance-covariance matrix are required. This estimation is usually done by classic estimators. However, they have some shortcomings, including their high sensitivity to outlier data. Changes, trends, and outliers in Phase I data have an undesirable impact on the performance of control charts in Phase II. This makes the control limits wider, which increases the type I error and reduces the power in detecting assignable causes in Phase II. To deal with these outliers, different methods have been used, among which robust estimators are one of the most widely used. These estimators are resistant to outliers and provide a better estimation of the parameters (Montgomery et al, 2015) (Huber, 1981). These estimators have been used by many researchers in developing different Hotelling's T^2 control charts. (Williams et al, 2006) showed that the classic sample covariance-matrix estimator is not effective in detecting process changes, and proposed a more effective estimator based on sequential data differences. Using minimum covariance determinant (MCD) and minimum volume ellipse (MVE), (Vargas, 2006) proposed a robust control chart for multivariate individual observations and determined the control limits experimentally. (Jensen et al, 2007) used MCD and MVE estimators to design a Phase-I T^2 control chart for individual observations. (Variyath and Steiner, 2009) proposed a robust Hotelling's T^2 control

chart for individual observations in Phase II by using a re-weighted minimum covariance determinant (RMCD) estimator. (Alfaro and Ortega, 2009) compared the behavior of different robust Hotelling's T^2 control charts developed by the MCD, MVE, RMCD, and trimmed estimators. (Yanez et al, 2010) proposed a robust Hotelling's T^2 control chart for multivariate individual observations based on Tukey's biweight function. (Abu-Shawiesh et al, 2014) compared the performance of two-variable Hotelling's T^2 control chart based on MCD, MVE, and MEDMad estimators in monitoring individual observations. (Wu et al, 2017) evaluated the properties and enhancements of robust likelihood CUSUM control charts in monitoring the mean of contaminated normally distributed processes. (Nasir, 2019) proposed a robust S^2 control chart for the case where the unknown parameters are estimated by Phase-I samples. (Maleki et al, 2020) proposed a T^2 control chart using median-based estimators. Control charts are also widely used in healthcare areas. They are specifically beneficial in diagnosing cancer tumors and metastases in medical images since their early and in-time diagnosis is of special importance. However, the method used always for the final diagnosis is pathobiology. Despite the capability in diagnosing different types of diseases, it has some problems such as its aggressiveness (need to sample), relatively long response time, and the results whose interpretation is dependent on the experience of the pathologist (Crow et al, 2003). To overcome these deficiencies, several techniques have been proposed in the past years. Among these methods,

*Corresponding author Email address: amirhossein.amiri@gmail.com

magnetic resonance imaging (MRI) techniques, due to their non-aggressive and non-destructive nature in providing multispectral images, have been of special interest. Due to the complexity of body tissues, the manual detection of tissues like those of the pelvic region and metastases is time-consuming and depends on the conditions of the operator. Besides, the need for experts who can diagnose these is vital and makes the usual and old methods inefficient in the absence of such experts. To overcome this, the use of computer-aided medical image processing techniques and algorithms is very helpful. In this regard, some useful works have been done on different methods of feature extraction, classification, and clustering. (Rouhi et al, 2015) proposed two automatic methods for diagnosing benign and malignant breast tumors in mammography. In the first one, the classification was based on an automated region growing whose threshold was obtained by a trained artificial neural network (ANN). In the second one, the samples were classified by a cellular neural network (CNN) whose parameters were determined by a genetic algorithm (GA). (Öztürk and Akdemir, 2018) compared the results obtained from different feature extraction and classification methods for histopathological images. They used the Gray-Level Co-Occurrence Matrix (GLCM), Local Binary Patterns (LBP), Local Binary Gray Level Co-occurrence Matrix (LBGLCM), Gray Level Run Length Matrix (GLRLM), and Segmentation-based Fractal Texture Analysis (SFTA) for feature extraction, and Support Vector Machine (SVM), K-nearest neighbors (KNN), linear discriminant analysis (LDA), Boosted Tree for the classification. (Al Ghayab et al, 2018) proposed a new feature extraction technique based on tunable Q-factor wavelet transform (TQWT) for the analysis of electroencephalograms (EEGs). To evaluate their proposed technique, they transmitted the extracted features to a bagging tree (BT), k nearest neighbor (K-NN), and support vector machine (SVM). To diagnose patients suspected of bone marrow metastasis, (Shahrabi et al, 2019), (Shahrabi et al, 2020) used a control chart using wavelet transformation, fuzzy clustering, and GA for feature extraction, classification, and selection. (Maharjan et al, 2020) used convolutional deep neural networks (CNN) to improve the classification accuracy and support multi-class classification. Using a hybrid deep auto-encoder, (Raja et al, 2020) segmented brain tumors by a Bayesian fuzzy clustering approach. (Hashemzahi et al, 2020) applied a hybrid model of CNN and neural autoregressive distribution estimation (NADE) methods to detect brain tumors in MRI images.

In this paper, due to the interdependence of the extracted features and the need for their simultaneous control, we propose a new robust Hotelling's T^2 control chart instead of the usual methods of the literature (clustering and classification methods). The proposed robust control chart, which is not much sensitive to outlier data, is designed based on the non-metastasized data in Phase I. Then, by adding bone marrow metastasized samples (local contamination) and introducing different shifts in the mean, we compare the ARL performance of the classic and robust methods in Phase II.

The remainder of this paper is organized as follows. In Section 2, the proposed methodology is described step by step. Section 3 includes the simulation studies and the results. Section 4 provides a discussion and analysis of the results. Finally, in Section 5, the paper is concluded and some research areas are suggested.

2. Proposed Method

Fig. 1 illustrates our proposed methodology. We describe its steps here in detail.

2.1. Image acquisition

The proposed methods are applied to ADC (Apparent diffusion coefficient), T1-weighted with resolution 256×256 , digital imaging and communications in medicine (DICOM) format, and 16-bit MRI images of a healthy person and a patient with breast cancer or bone marrow metastasis in the pelvic region.

2.2. Two-dimensional discrete wavelet transformation

Wavelet transformation is one of the most powerful techniques in texture analysis. It does this by decomposing a texture image into a set of frequency channels. There are two wavelet structures (Garnavi et al, 2010): 1) pyramid-structured wavelet transform, which is out of our scope; and 2) tree-structured wavelet analysis, which makes possible the decomposition of the low, medium, and high frequencies. In the analysis of MRI images from the pelvic region, low-frequency components provide information about the general characteristics (shape), which are important clinically, and high-frequency components provide information about the texture details and region of interest, which are important for correct diagnosis. Thus, the decomposition of all ranges of frequency is helpful for this purpose. In this regard, tree-structured wavelet analysis can be more appropriate for this research. The low-frequency spectrum is the approximation signal and the high-frequency spectrum is the detail signal (Beylkin et al, 1991). Therefore, the wavelet transformation of an image with $M \times N$ resolution is

$$W_{\phi}(j_0, m, n) = \frac{1}{\sqrt{MN}} \sum_{x=0}^{M-1} \sum_{y=0}^{N-1} f(x, y) \phi_{j_0, m, n}(x, y), \quad (1)$$

$$W_{\psi}^i(j, m, n) = \frac{1}{\sqrt{MN}} \sum_{x=0}^{M-1} \sum_{y=0}^{N-1} f(x, y) \psi_{j, m, n}^i(x, y), \quad (2)$$

$i = \{ H, V, D \}$

, where j_0 is an arbitrary initial scale and $W_{\psi}^i(j, m, n)$ collects horizontal, vertical, and diagonal details for scales $j \geq j_0$. We usually set $j_0=0$ and select $N=M=2^J$ such that $j=0, 1, \dots, 2^{J-1}$ and $m=n=0, 1, \dots, 2^j$. Thus, the proposed method of this research is based on a two-dimensional wavelet transform. To obtain this two-dimensional transform, we perform a one-dimensional transform on the rows and columns of the image matrix and combine the elements of the two transformed matrices. Fig. 2 displays this process.

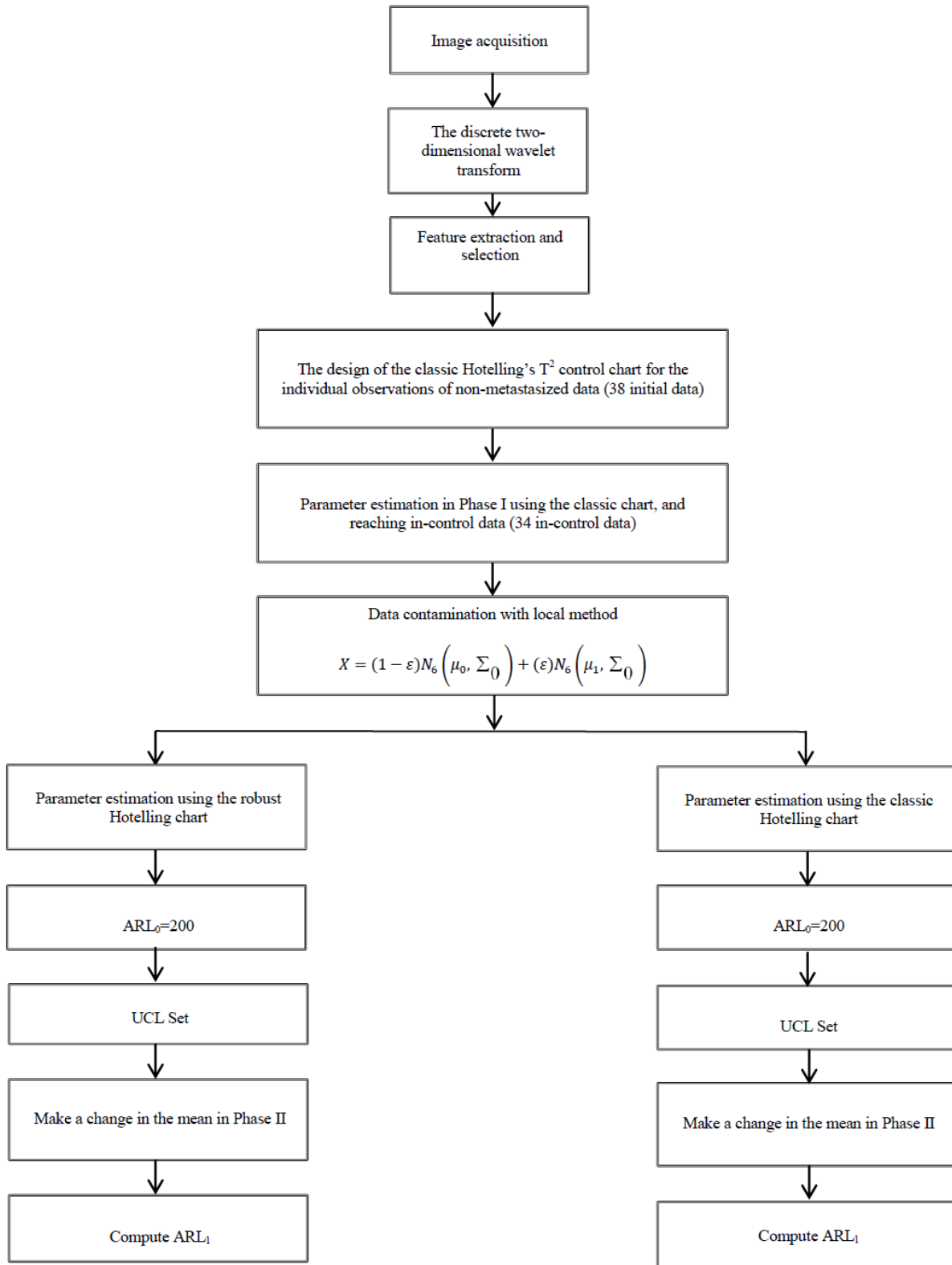


Fig. 1. The schematic diagram of the proposed method

2.3. Feature extraction and selection

In recent years, texture analysis has played an important role in different applications, especially in analyzing medical images. Texture features are used for the diagnosis and discrimination between the different textures of medical images. For this, two types of features are extracted from images: energy and histograms of oriented

gradients (HOG). The energy has three features: horizontal channel energy, vertical channel energy, and the energy of the image itself (Walvick et al, 2004). The second group of features includes 16 types of features (we describe them later). First, by applying the wavelet transform, each input image is transformed into a wavelet space. Then, the energy and the HOG at each component of the image are

calculated. Accordingly, the image's energy is calculated as follows:

$$P(i,j) = \frac{h(i,j)}{NM}, \quad i = 0,1,\dots,G-1, \quad j = 0,1,\dots,G-1 \quad (3)$$

$$(\text{Energy}): \sum_{i=0}^{G-1} \sum_{j=0}^{G-1} [p(i,j)]^2, \quad (4)$$

, where $P(i,j)$ is the probability density of occurrence of the intensity levels, $h(i,j)$ is the value of intensity level histogram, NM is the total number of pixels, with M as the resolution at the vertical axis and N at the horizontal axis, and G is the total grey level of the image (Ain et al, 2014). HOG was first introduced by (Dalal and Triggs et al, 2005). The gradient of an image is easily calculated by filtering the intensity data and using two one-dimensional filters along the x and y axes, $[-1,0,1]$ and $[-1,0,1]^T$ (Cai et al, 2018):

$$\nabla f(x,y) = \left(\frac{\partial f(x,y)}{\partial x}, \frac{\partial f(x,y)}{\partial y} \right), \quad (5)$$

where

$$\frac{\partial f(x,y)}{\partial x} = \frac{f(x+1,y)-f(x-1,y)}{(x+1)-(x-1)}, \quad (6)$$

$$\frac{\partial f(x,y)}{\partial y} = \frac{f(x,y+1)-f(x,y-1)}{(y+1)-(y-1)}, \quad (7)$$

To define $G_x = \frac{\partial f(x,y)}{\partial x}$ and $G_y = \frac{\partial f(x,y)}{\partial y}$, the amplitude and orientation of each pixel are given as follows:

$$|\nabla f(x,y)| = \sqrt{G_x^2 + G_y^2}, \quad (8)$$

$$\theta(x,y) = \tan^{-1} \left(\frac{G_y}{G_x} \right). \quad (9)$$

John proposed two methods for feature selection: the filtering method, which uses no classification functions and is out of the scope of this research; and the wrapper method, known as the black-box method, which uses a classification function for the fitness evaluation of the feature subset. In this paper, a genetic algorithm (GA) has been used for searching valid features since it can do a random search and is not prone to get stuck in a local minimum (Mitchell, 1996),(Jarmulak and Craw, 1999). In this stage, after applying the two-dimensional wavelet transform on the overall image, the Demy wavelet transform is used for texture analysis. To have the features of the region of interest, 76 features (19 ones from each of the four images obtained in the previous stage) were extracted from the images of the pelvic region. First, we took a two-dimensional gradient of the wavelet and calculated its energy one time along the x -axis and one time along the y -axis, and obtained the energy of the wavelet image as well. Then, we calculated the angle between the horizontal and vertical gradients (from $-\pi$ to π divided by 16) and took its normalized histogram. That is, we took the oriented gradient and calculated its histogram. Those 16 angles were considered as the histogram boundaries, resulting in 16 normalized histograms with a probability between 0 and 1. Next, we calculated 19 (16 + 3) features for each one of the approximation channel I_{LL} , horizontal channel I_{LH} , vertical channel I_{HL} , and diagonal channel I_{HH} , and extracted the similarity matrix from the comparison of the extracted features. Finally, using the GA, whose objective is to obtain the minimum value (a chromosome with the minimum weighted sum of the features), six features were selected (Rouhi et al, 2015), (Shahrabi et al, 2020).

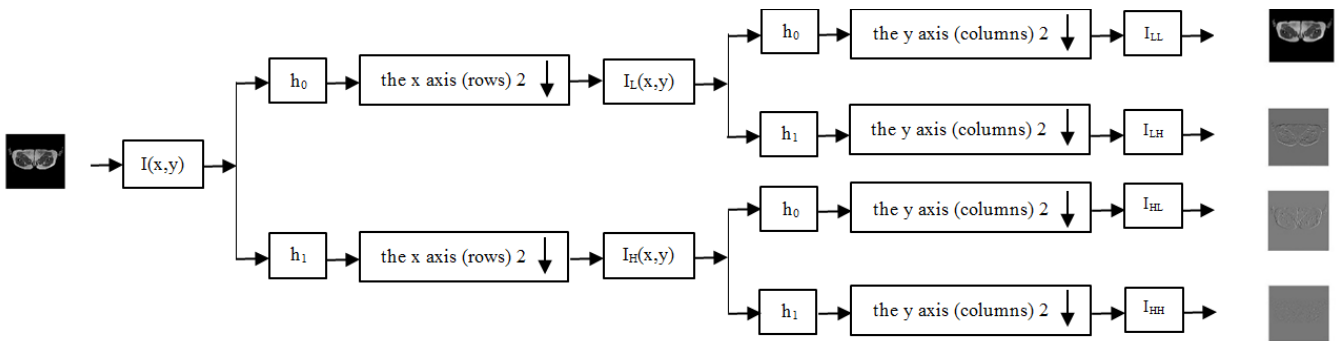


Fig. 2. The block diagram of the discrete two-dimensional wavelet transform

2.4. The design of the control chart and parameter estimation in Phase I

First, using the classic Hotelling's T^2 control chart, a control chart is designed for the individual observations for the non-metastasized data (38 initial data). Then, by estimating the parameters, calculating the control limits, and obtaining in-control data (34 in-control data), the final control chart is designed.

2.5. Contaminating the data

Two types of data contamination are possible: global and local. Local contamination affects the data of one or multiple sub-groups (Maronna et al, 2006). It is assumed

that, with probability ε , some data have a distribution different from the basic distribution. The data generated from this different distribution are contaminated data or outliers. If X comes from a process that has distribution $G(x)$ with probability $(1-\varepsilon)$ and has distribution $H(x)$ with probability ε , it has the following combined distribution:

$$F(x) = (1 - \varepsilon)G(x) + \varepsilon H(x), \quad (10)$$

A special type of contamination is when the density functions $G(x)$ and $H(x)$ are both normal. In this case, data follows a contaminated normal distribution. Therefore, whenever only local contamination exists in the process, the density function of the output is a contaminated normal distribution with the following combined density:

$$X = (1 - \varepsilon)N_6(\mu_0, \Sigma_0) + \varepsilon N_6(\mu_1, \Sigma_0), \quad (11)$$

Global contamination, on the other hand, refers to contamination that occurs with an equal probability for all data. It is out of our scope. In this paper, for data contamination, we used 10 metastasized data inserted into the non-metastasized data (34 data) with four different frequencies: two data (5% contamination), four data (10% contamination), seven data (20% contamination), and 10 data (30% contamination).

2.6. Parameter estimation in Phase II and ARL₁ calculations

The average run length (ARL) is one of the most widely used and valid measures in evaluating control charts in Phase II. It is the average of the points plotted on a chart until a point places out of the control limits. Thus, in control and out of control ARL values are calculated by

$$ARL_0 = \frac{1}{\alpha}, \quad (12)$$

$$ARL_1 = \frac{1}{1 - \beta},$$

respectively.

After introducing the contamination into the data, for both the classic and robust Hotelling's control charts, we estimate the parameters, calculate ARL₀, set UCL, introduce a shift in the mean, and calculate the ARL₁.

2.7. The robust Hotelling's T² control chart

Hotelling's control chart is the most famous for monitoring the mean vector of multivariate processes. Control charts are designed in two phases. The objective of the first phase is to achieve a dataset of in-control data. Assuming that the process has been in-control in Phase I, it is evaluated to see whether the process is in-control or not in Phase II using new observations. However, the existence of outlier data in Phase I can have a non-desirable effect on the control limits of Phase II. These data are the contaminated data that dramatically affect classic estimators. Instead of removing outliers, it is better to use robust estimators for parameter estimation. The control charts based on this concept, which was first introduced by Box (Box, 1979), have the required sensitivity for detecting out-of-control states although they are subject to outlier data. (Williams et al, 2006) showed that classic estimators of the sample variance-covariance matrix are not effective in detecting process changes. Thus, they proposed the use of the

difference between the successive observations ($v_i = x_{i+1} - x_i, i = 1, 2, \dots, n-1$) for the estimation of the covariance matrix. The location and dispersion estimators for this method are:

$$T_j^2 = (\mathbf{x}_j - \bar{\mathbf{X}})' \mathbf{S}^{-1} (\mathbf{x}_j - \bar{\mathbf{X}}), \quad (13)$$

$$\bar{\mathbf{X}} = \frac{1}{n} \sum_{j=1}^n \mathbf{x}_j, \quad (14)$$

$$\mathbf{S} = \frac{1}{2(n-1)} \sum_{i=1}^{n-1} \mathbf{v}_i \mathbf{v}_i', \quad (15)$$

Finally, they showed that the T² control chart with the sample mean vector and mean square vector of successive differences has the highest sensitivity in detecting mean changes. (Masson and Yang, 1946) considered the following Phase I control limits of the T² control chart for individual observations:

$$UCL = \frac{(m-1)^2}{m} \beta_{\alpha, \frac{p}{2}, \frac{(m-p-1)}{2}} \quad (16)$$

$$LCL=0$$

, where $\beta_{\alpha, \frac{p}{2}, \frac{(m-p-1)}{2}}$ is the α^{th} value of the Beta

distribution. It should be noted that parameter **S** of the classic estimators in Eq. (13) (the sample variance-covariance matrix) should be replaced by the following covariance matrix (Keramatpour et al, 2014).

$$\mathbf{S} = \frac{1}{n-1} \sum_{i=1}^{n-1} \mathbf{v}_i \mathbf{v}_i', \quad (17)$$

3. Simulation Studies And Results Analysis

In this section, we evaluate the performance of the classic (sample variance-covariance matrix) and robust (Williams et al.) methods in detecting different shifts, different changes in the mean of different variables, and different contamination percentages. We used a multivariate control chart model in the simulation studies. We used six features of the ones extracted from the MRI images of ADC and T₁ of the pelvic region. In the model, the features of the non-metastasized bone marrow cases (i.e. those who have primary breast tumors but do not have bone marrow metastasis) were monitored. Therefore, the values of the model variables for the multivariate control chart are as shown in Table 1.

Table 1
The initial values of the model variables

Row	X ₁	X ₂	X ₃	X ₄	X ₅	X ₆
1	5.919813946	0.02142874	0.064178588	0.131176561	0.062569547	0.066665996
2	5.869353826	0.030231337	0.073042113	0.11271181	0.048385115	0.066329435
3	5.841597042	0.039201508	0.060010829	0.112002221	0.057397257	0.053778866
4	5.847457199	0.045593849	0.066435405	0.104525783	0.04844576	0.070884468
5	5.826309248	0.046361829	0.054041111	0.123612372	0.058966878	0.067518893

6	5.844333553	0.05788451	0.063719281	0.111000031	0.058785578	0.064514142
7	5.92015725	0.043748337	0.075802638	0.11343288	0.05649185	0.055402921
8	5.850744704	0.041706905	0.057791863	0.131724219	0.056535296	0.085313156
9	5.872261135	0.047537117	0.06226029	0.107251676	0.057328182	0.067971312
10	5.846610505	0.038093417	0.072754004	0.095286344	0.047693571	0.065446348
11	5.864832954	0.03589725	0.059443323	0.131945799	0.056616337	0.075599691
12	5.905473213	0.05565261	0.070437816	0.085590351	0.042757914	0.056330412
13	5.884325897	0.044375049	0.057998885	0.119320553	0.052928806	0.072077184
14	5.820621814	0.035500277	0.057656086	0.138989187	0.055736399	0.055223491
15	5.877048536	0.046144386	0.060402796	0.109395234	0.061813528	0.063688683
16	5.781977943	0.02622502	0.063680216	0.140805198	0.066562435	0.048396266
17	5.8173167	0.049059666	0.045761225	0.113384879	0.032804197	0.06870885
18	5.692943267	0.047202488	0.054539942	0.106845756	0.064734929	0.073203687
19	5.750525058	0.034888683	0.054098726	0.119582478	0.04132866	0.077804754
20	5.84689565	0.022970202	0.044857918	0.138617898	0.059701893	0.066159541
21	5.711903156	0.044838296	0.048245872	0.132917952	0.05093953	0.073088146
22	5.850986619	0.03922384	0.075302982	0.105327841	0.068966186	0.079682747
23	5.854795707	0.036322732	0.044446413	0.12619151	0.055247337	0.095324885
24	5.777463257	0.054068992	0.060174718	0.10173152	0.052874249	0.078135068
25	5.777542277	0.047176119	0.068657151	0.091106438	0.058097416	0.082133973
26	5.772785925	0.063702124	0.061347731	0.101411477	0.047809382	0.067708643
27	5.824385442	0.041061926	0.043022865	0.101730225	0.051220505	0.079115023
28	5.765395263	0.03587255	0.052065922	0.129892151	0.063159129	0.07147278
29	5.7333196	0.067682085	0.061340866	0.099975748	0.048997139	0.07702632
30	5.731926419	0.041800998	0.06496847	0.119846423	0.077881845	0.082958883
31	5.715501029	0.033046301	0.060256249	0.10956261	0.058897602	0.071211671
32	5.699493677	0.044308017	0.031293694	0.121470456	0.048183076	0.085733897
33	5.77010524	0.03939764	0.051090522	0.114833332	0.042489126	0.076140183
34	5.919627265	0.039503385	0.075028654	0.142293041	0.069474408	0.068261133
35	5.764294385	0.045982275	0.047116568	0.122731014	0.075548337	0.051434953
36	5.807337803	0.028870428	0.036133437	0.096864257	0.058200383	0.080223086
37	5.704451638	0.047222793	0.065998095	0.078100768	0.034785324	0.08791703
38	5.922324515	0.020292981	0.026883375	0.116562095	0.053740563	0.057436184

Using R software, we design a classic Hotelling control chart for the individual data for the metastasized data given in Table 1 (38 initial data). Then, by estimating the parameters and having data within an in-control state, the final control chart (34 in-control data) is developed. Then, to have locally contaminated data, we add the bone marrow metastasized data to the in-control chart and performed the simulation studies in MATLAB software. To introduce some shifts into the parameters, we considered the range from 0.01 to 0.1 with step 0.01. In this research, the number of the bone marrow metastasized samples is denoted by ε , which determines the percentage of contamination in the data (0%, 5%, 10%, 20%, and 30%). The control limits of the proposed methods obtained by 10000 simulation runs for an $ARL_0=200$ are given in Table 2. The ARL_1 results display the ability of the robust

Hotelling's T^2 control chart in detecting the changes made in the parameters.

Based on the literature of robust control charts, the performance of the control charts depends on the identification of outliers in Phase I. That is, if the number of outliers and contaminated data increase, the estimates will be more accurate, and as a result, the control chart performance improves. Accordingly, in this paper, we evaluated the performance under different percentages of contamination. According to these percentages, we considered respectively 0, 2, 4, 7, and 10 outlier data. The simulation results in Tables 2, 3, and 4, which respectively show the changes in one, two, and all the six variables, indicate that the performance of the robust control chart improves for the higher values of ε and gives out-of-control signals sooner.

Table 2

The ARL_1 values of the classic and robust control charts in detecting the changes introduced into the mean of one variable

Percent of Contamination	UCL	Control Chart	d									
			0.01	0.02	0.03	0.04	0.05	0.06	0.07	0.08	0.09	0.100
0%	18.57 5	Classic T^2	196.60	168.69	141.94	111.45	82.69	61.52	46.11	33.84	23.85	18.09
	27.59 5	Robust T^2	188.03	163.34	130.83	100.35	74.57	55.91	41.34	30.69	22.69	17.42
5%	16.86 5	Classic T^2	196.78	196.49	193.61	188.38	182.66	172.94	166.38	160.46	151.31	139.64
	19.85	Robust T^2	194.41	191.71	185.42	175.24	167.09	159.20	148.41	141.20	130.15	120.14

	8											
10%	17.39 9	Classic T ²	197.75	195.89	189.64	187.59	179.68	170.09	165.03	157.84	150.58	138.90
	20.65 0	Robust T ²	190.83	183.92	175.63	162.58	153.44	138.39	130.43	118.31	111.78	99.42
20%	18.04 9	Classic T ²	196.73	195.34	189.56	188.99	178.39	170.96	165.79	157.98	148.51	139.78
	23.33 5	Robust T ²	186.06	171.97	161.59	145.88	134.26	120.34	111.14	98.07	86.93	76.68
30%	18.19 0	Classic T ²	198.73	194.51	187.24	179.09	176.74	171.33	157.59	149.46	142.11	132.44
	25.14 6	Robust T ²	179.49	164.48	147.96	131.18	114.99	102.11	88.24	77.58	65.56	58.60

It is obvious that for all values of ϵ , the robust control chart outperforms significantly the classic chart in detecting the

small, medium, and large shifts in the mean of one variable.

Table 3

The ARL₁ values of the classic and robust control charts in detecting the changes introduced into the mean of two variables.

Percent of Contamination	UCL	Control Chart	<i>d</i>										
			0.01	0.02	0.03	0.04	0.05	0.06	0.07	0.08	0.09	0.100	
0%	18.575	Classic T ²	44.78	5.87	1.69	1.08	1.00	1.00	1.00	1.00	1.00	1.00	1.00
	27.595	Robust T ²	73.92	11.40	2.53	1.23	1.02	1.00	1.00	1.00	1.00	1.00	1.00
5%	16.865	Classic T ²	42.53	5.84	1.73	1.09	1.01	1.00	1.00	1.00	1.00	1.00	1.00
	19.858	Robust T ²	55.92	7.96	2.11	1.17	1.01	1.00	1.00	1.00	1.00	1.00	1.00
10%	17.399	Classic T ²	41.97	5.93	1.74	1.10	1.01	1.00	1.00	1.00	1.00	1.00	1.00
	20.650	Robust T ²	53.58	7.63	2.08	1.16	1.01	1.00	1.00	1.00	1.00	1.00	1.00
20%	18.049	Classic T ²	46.25	6.44	1.81	1.11	1.01	1.00	1.00	1.00	1.00	1.00	1.00
	23.335	Robust T ²	66.80	9.26	2.34	1.21	1.02	1.00	1.00	1.00	1.00	1.00	1.00
30%	18.190	Classic T ²	54.13	7.87	2.07	1.15	1.01	1.00	1.00	1.00	1.00	1.00	1.00
	25.146	Robust T ²	67.74	11.09	2.69	1.28	1.03	1.00	1.00	1.00	1.00	1.00	1.00

In detecting the changes in two variables, with the increase of ϵ , the classic control chart only performs better for the small shifts while both control charts have the same performance for the medium and large shifts.

Finally, according to Table 4, for all values of ϵ , the robust and classic control methods have the same performance in detecting the changes made in all six variables.

4. Discussion

To be comparable, control charts are generally designed such that their type I error, equivalently their ARL₀ values is almost equal. In this way, the control chart that is more sensitive in detecting out-of-control states is more desirable. In other words, for a certain change in the

process parameters, the chart with probability of type II error (smaller ARL₁s) is more desirable since it detects out-of-control states sooner on average. Accordingly, we evaluated the ARL₁ performance of the robust and classic control charts when there is local contamination. We did this for different changes made in the mean of one, two, and all six variables of the process. The results, in general (for example, those illustrated in Figs 4 and 5) confirm the better performance of the robust version.

As can be seen, in the case of contamination in the Phase I data, the performance of both charts is almost the same in Phase II (for the changes in the mean of one variable).

Table 4

The ARL_1 values of the classic and robust control charts in detecting the changes introduced into the mean of all six variables.

Percent of Contamination	UCL	Control Chart	d									
			0.01	0.02	0.03	0.04	0.05	0.06	0.07	0.08	0.09	0.100
0%	18.575	Classic T^2	4.09	1.02	1.00	1.00	1.00	1.00	1.00	1.00	1.00	1.00
	27.595	Robust T^2	6.83	1.06	1.00	1.00	1.00	1.00	1.00	1.00	1.00	1.00
5%	16.865	Classic T^2	3.35	1.01	1.00	1.00	1.00	1.00	1.00	1.00	1.00	1.00
	19.858	Robust T^2	3.68	1.02	1.00	1.00	1.00	1.00	1.00	1.00	1.00	1.00
10%	17.399	Classic T^2	3.29	1.01	1.00	1.00	1.00	1.00	1.00	1.00	1.00	1.00
	20.650	Robust T^2	3.64	1.02	1.00	1.00	1.00	1.00	1.00	1.00	1.00	1.00
20%	18.049	Classic T^2	3.39	1.02	1.00	1.00	1.00	1.00	1.00	1.00	1.00	1.00
	23.335	Robust T^2	4.75	1.03	1.00	1.00	1.00	1.00	1.00	1.00	1.00	1.00
30%	18.190	Classic T^2	4.32	1.03	1.00	1.00	1.00	1.00	1.00	1.00	1.00	1.00
	25.146	Robust T^2	8.43	1.09	1.00	1.00	1.00	1.00	1.00	1.00	1.00	1.00

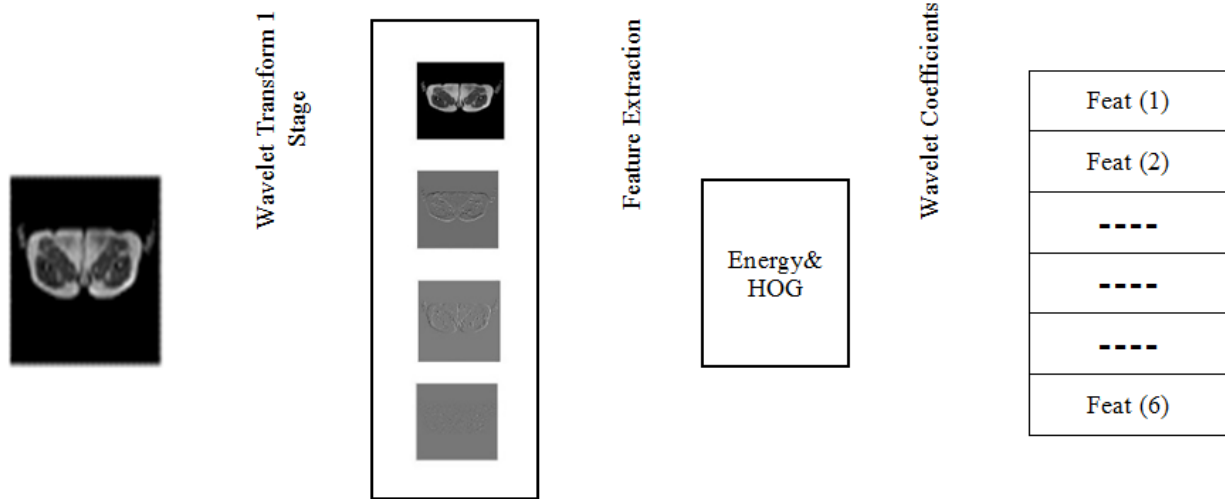


Fig. 3. The schematic diagram of the extracted, and then selected features

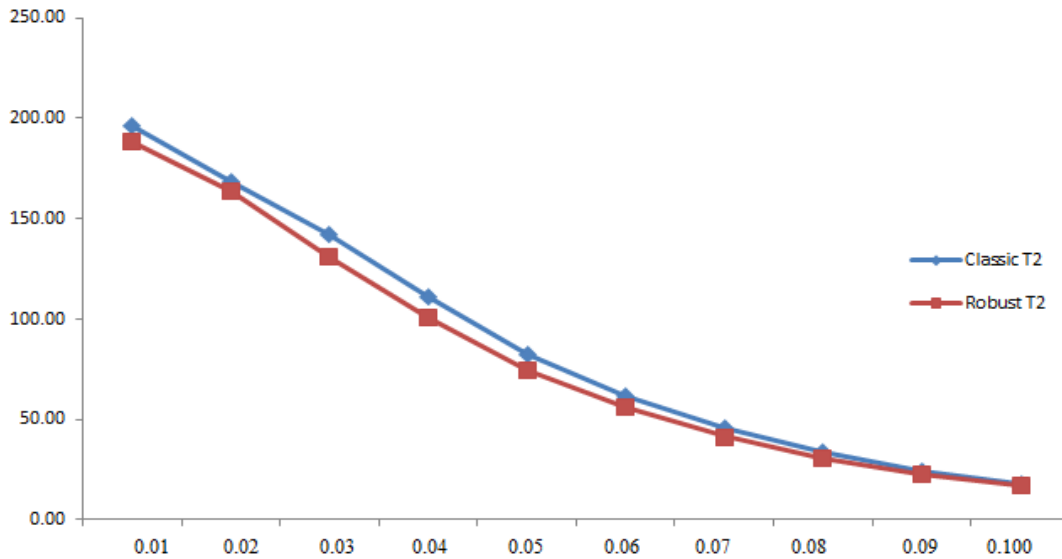


Fig. 4. The ARL₁ values for the classic and robust Hotelling's T² control charts with ε=0%.

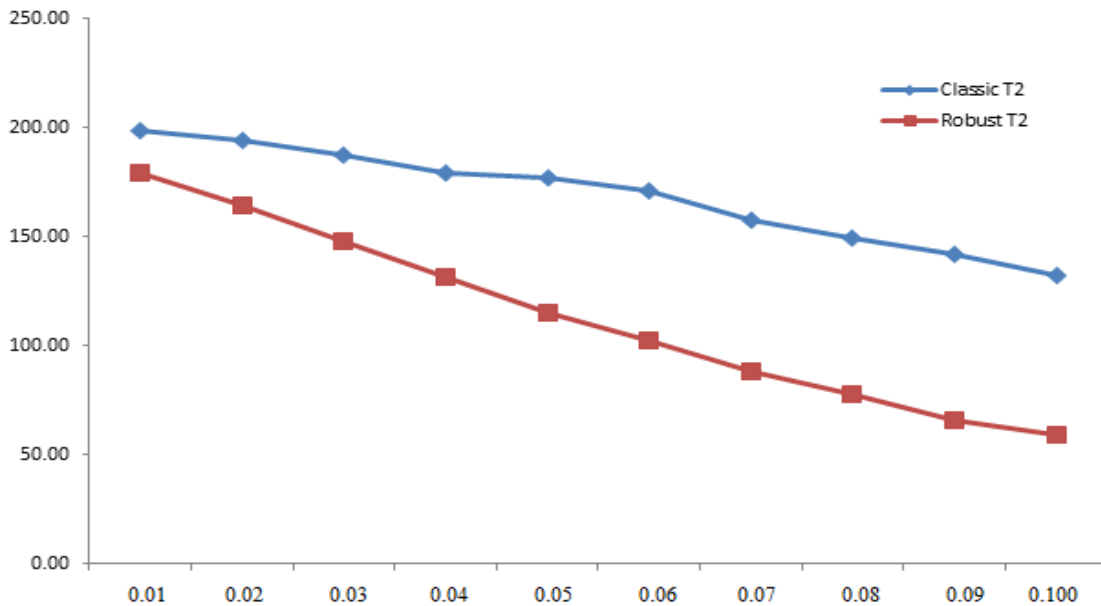


Fig. 5. The ARL₁ values for the classic and robust Hotelling's T² control charts with ε=30%.

As can be seen in Fig. 5, in the case of contamination in the Phase I data, the robust control chart has a better performance than the classic one in Phase II (for the changes in the mean of one variable).

5. Conclusion And Suggestions For Future Research

In this paper, we proposed a procedure based on multivariate control charts for the diagnosis of bone marrow metastasis in medical images. Then, we designed a classic and a robust Hotelling's T² control chart for the monitoring of patients suspected of bone marrow metastasis in the pelvic region. The proposed control charts

have acceptable performance in parameter estimation under the presence of contaminated data. These estimators are robust estimators of the mean vector and variance-covariance matrix. We evaluated the ARL₁ performance of the classic and robust control charts in detecting changes of different magnitudes in the mean of different variables and under different percentages of data contamination. The simulation results showed that the robust method had a better performance than the classic one. In this research, for the first time, instead of traditional clustering and classification methods, a multivariate control chart with Hotelling T² statistic was used for bone marrow diagnosis of people suspected to bone marrow metastasis. This

robust method, which has low sensitivity to outliers, can simultaneously control the interdependent features. For further research in this context, the development of self-starting robust and fuzzy self-starting control charts, the use of other robust estimators instead of the proposed method, and the use of skewed and non-normal distributions for the contaminated data can be some potential areas.

References

- Montgomery, D. C., Peck, & E. A. Vining, G. (2015). Introduction to linear regression analysis (4th ed.), John Wiley & Sons, New York.
- Huber, P. J. (1981). Robust Statistics, John Wiley & Sons, New York.
- Williams, J. D., Woodall, W. H., Birch, J. B. and Sullivan, J. H. (2006). On the Distribution of Hotelling's T^2 Statistic based on the Successive Difference Covariance Matrix Estimator. *Journal of Quality Technology*, 38(3), 217-229.
- Vargas, N. J. A. (2003). Robust Estimation in Multivariate Control Chart for Individual Observations. *Journal of Quality Technology*, 35(4), 367-376.
- Jensen, W. A., Birch, J. B. and Woodall, W. H. (2007). High Breakdown Estimation Methods for Phase I Multivariate Control Charts. *Quality and Reliability Engineering International*, 23(5), 615-629.
- Chenouri, S. E., Steiner, S. H., Variyath, A. M. (2009). A Multivariate Robust Control Chart for Individual Observations. *Journal of Quality Technology*, 41(3), 259-271.
- Alfaro, J. L. and Ortega J. F. (2009). A Comparison of Alternative to the Hotelling's T^2 Control Chart. *Journal of Applied Statistics*, 36(12), 1385-1396.
- Yanez, S., Gonzalez, N. and Vargas, J. A. (2010). Hotelling's T^2 Control Charts based on Robust Estimators. *Dyna*, 77(163), 239-247.
- Abu-Shawiesh, M. O. A., Kibria, G. and George, F. (2014). A comparison of some Robust Bivariate Control Chart for Individual Observations. *International Journal for Quality Research*, 8(2), 183-196.
- Wu, C., Yu, M. and Zhuang, F. (2017). Properties and enhancements of robust likelihood CUSUM control chart. *Computers & Industrial Engineering*, Vol. 114(C), 80-100.
- Nasir, A. (2019). A robust S2 control chart with Tukey's and MAD outlier detectors, *Quality and Reliability Engineering International*, 31(1), 403-413.
- Maleki, F., Mehri, S., Aghaie, A., Shahriari, H. (2020). Robust T^2 control chart using median-based estimators. *Quality and Reliability Engineering International*, 36(6), 2187-2201.
- Crow, P., Stone, N., Kendall, C.A., Persad, R.A., Wright M.P.J. (2003). Optical diagnostics in urology: current applications and future prospects. *BJU International*, 92(4), 400-407.
- Rouhi R., Jafari M., Kasaei S., Keshavarzian P. (2015). Benign and malignant breast tumors classification based on region growing and CNN segmentation, *Expert Systems with Applications*, 42(3), 990-1002.
- Ozturk, S., Akdemir, B. (2018). Application of feature extraction and classification methods for histopathological image using GLCM, LBP, LBGLCM, GLRLM and SFTA, *Procedia Computer Science*, 132, 40-46.
- Al Ghayab, H.R., Li, Y., Siuly, S., Abdulla, S. (2018). A feature extraction technique based on tunable Q-factor wavelet transform for brain signal classification, *Journal of Neuroscience Methods*, *Journal of Neuroscience Methods*, 312(1), 43-52.
- Shahrabi, M., Amiri, A., Saligheh Rad, H., Ghofrani, S. (2019). Design of Multivariate Hotelling's T^2 Control Chart Based on Medical Images Processing, *Iranian Journal of Radiology*, 16(Special Issue):e99146., DOI : 10.5812/iranjradiol.99146.
- Shahrabi, M., amiri, A., Saligheh Rad, H., Ghofrani, S. (2020). The Diagnosis of Patients Suspected to Bone Marrow Metastasis based on Multivariate Control Chart, *Published online in International Journal of Hospital Research*.
- Maharjan, S., Alsadoon, A., Prasad P.W.C. and Alsadoon, O.H. (2020). A novel enhanced softmax loss function for brain tumour detection using deep learning, *Journal of Neuroscience Methods*, 330(1), 1-11.
- Raja, S., P.M., Rani and Viswasa, A. (2020). Brain tumor classification using a hybrid deep autoencoder with Bayesian fuzzy clustering-based segmentation approach, *Biocybernetics and Biomedical Engineering*, 40(1), 440-453.
- Hashemzahi, R., Mahdavi, S.J., Kheirabadi, M., Kamel, S.R. (2020). Detection of brain tumors from MRI images base on deep learning using hybrid model CNN and NADE, *Published online in Biocybernetics and Biomedical Engineering*, doi: 10.1016/j.bbe.2020.06.001.
- Garnavi, R., Aldeen, M., Bailey, J. (2010). Classification of Melanoma Lesions Using Wavelet-Based Texture Analysis, *International Conference on Digital Image Computing: Techniques and Applications*, Sydney, NSW, Australia, IEEE.
- Beylkin, G., Coifman, R. and Rokhlin, V. (1991). Fast wavelet transforms and numerical algorithms I, *Communications on pure and applied mathematics*, 44(2), 141-183.
- Walvick, R. P., Patel, K., Patwardhan, S. V., & Dhawan, A. P. (2004). Classification of melanoma using wavelet-transform-based optimal feature set. In *Medical Imaging : Image Processing*, 5370(1), 944-952.
- Ain, Q., Jaffar, A., Choi, T. (2014). Fuzzy anisotropic diffusion based segmentation and texture based ensemble classification of brain tumor, *Applied Soft Computing*, 21(1), 330-340.
- Dalal, N. and Triggs, B. (2005). Histograms of oriented gradients for human detection, In *CVPR*.

- Cai, L., Zhu, J., Zeng, H., Chen, J., Cai, C., Ma, K. (2018). HOG-assisted deep feature learning for pedestrian gender recognition, *Journal of the Franklin Institute*, 355(1), 1991-2008.
- Mitchell, M. (1996). an introduction to genetic algorithms, MIT Press.
- Jarmulak, J., Craw, S. (1999). ears in Proceedings of the IJCAI'99 workshop on Automating the Construction of Case Based Reasoners.
- Maronna, R., Martin, D. and Yohai, V. (2006). Robust Statistics. John Wiley and Sons, England.
- Box, G. E. (1979). Robustness in Strategy of Scientific Model Building. Robustness in Statistics, 1st Edition.
- Mason, R.L., Young, J.C. (1946). Multivariate statistical process control with industrial application. Virginia ASA SIMA.
33. Keramatpour, M., Akhavan Niaki, S., Amiri, A. (2014). Phase-II Monitoring of AR (1) Autocorrelated Polynomial Profiles. *Journal of Optimization in Industrial Engineering*, 7(14), 53-59.

This article can be cited:

Shahrabi, M., Amiri, A., Saligheh Rad, H., Ghofrani, S. (2022). A New Method for Diagnosing Patients Suspected of Bone Marrow Metastasis in the Presence of Outliers. *Journal of Optimization in Industrial Engineering*, 15(1), 175-185.

http://www.qjie.ir/article_686435.html
DOI: 10.22094/joie.2021.1919440.1815

